MODELLING AND VERIFICATION OF MECHANICAL STRESS INDUCED BY SOLDERING OF WIRES FOR MULTI BUSBAR INTERCONNECTION

Li Carlos Rendler[1], Johann Walter[1], Torsten Geipel[1], Michael Volk[2], Christian Ebert[2], Ulrich Eitner[1]
[1]Fraunhofer Institute for Solar Energy Systems ISE, Heidenhofstraße 2, 79110 Freiburg, Germany
[2]SCHMID Group | Gebr. SCHMID GmbH, Robert-Bosch-Str. 32-36, 72250 Freudenstadt, Germany

ABSTRACT: The Multi Busbar metallization approach changes the interconnection architecture on silicon solar cells essentially. Compared to a standard H-pattern design with three continuous soldered busbars, between 7 and 15 round copper wires are soldered onto more than 200 solder pads on the front side of the solar cell. Due to the different coefficients of thermal expansion of copper and silicon, mechanical stress is induced after the interconnection. In this work we simulate the mechanical stress induced by soldering with a finite element model and experimentally verify the simulated results. The characterization of the stress distribution in the solder joints of a 78 by 10 mm² cell section shows that the cell bow, which is a visible indicator for mechanical stress, rises approximately from 4 to 9 mm when the wire diameter is increased from 250 to 430 µm. Pre-stretching the interconnecting wires up to 1% before soldering causes a slight increase of the cell bow. The verified simulation model allows the identification of reasons for potential defects of solder joints after reliability testing and the determination of the areas where such defects most likely occur. In addition, the model enables a comparison of the thermo-mechanical stress distribution of different interconnection concepts.

Keywords: FEM, Modelling, Multi Busbar, PV Materials, Wire Interconnection

1 INTRODUCTION

Crystalline silicon solar cells in standard solar modules are usually interconnected by soldering ribbons on the three busbars of the front- and back-side metallization. There are solar cells with other metallization designs available on the market, for example four and five busbar cells as well as the SmartWire Connection Technology of Meyer Burger, that uses a number of thin wires embedded in a polymer foil for the cell interconnection [1].

An innovative front-side metallization architecture is provided by the Multi Busbar (MBB) approach [2, 3, 4] as proposed by Schmid. MBB cells are interconnected by seven to fifteen solder coated copper wires with circular cross section (Diameter between 200 and 430 µm) on each side of the solar cell. The wires are soldered by infrared soldering on silver pads connecting five contact fingers respectively. Figure 1 shows the top view image of a solar cell metallization architecture for MBB interconnection with the screen printed and fired silver pad structure.

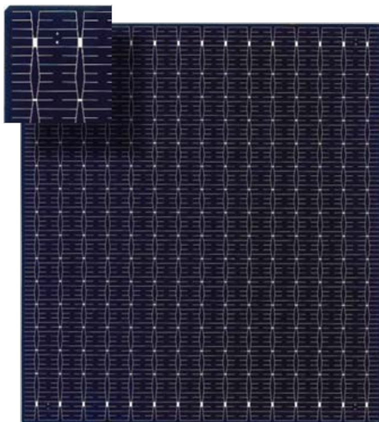

Figure 1: Top view image of a MBB solar cell with 15 pad rows and x-shaped redundancy fingers, connecting each solder pad to five contact fingers [2].

This layout and the MBB interconnection approach offers advantages compared to the standard H-pattern cell interconnection with three busbars: First, a more homogenous current collection from the cell area results in reduced series resistance and enables finer contact finger and busbar structures. This leads to reduced silver consumption and shading on the cell [2]. Second, the circular shape of the wires generates additional reflection gains on module level which enables reduced shading losses and results in higher module efficiencies [3].

However, the MBB approach requires the realization and reliability of over 200 solder joints on the front side and a number of solder joints on the back side of each solar cell. From the mechanical point of view this represents a major difference to the continuous soldering of a standard three busbar H-pattern design. As an example for a defect caused by thermo-mechanical stress, Figure 2 shows a cohesive fracture in the solder that occurred after temperature cycling according to DIN EN 61215 (-40 °C to 85 °C, 50 cycles) [5]. Besides, mechanical stress potentially induces delamination of the metallization paste or adhesive fracture between solder and silver paste. In some cases, combinations of the different defect mechanisms can be found.

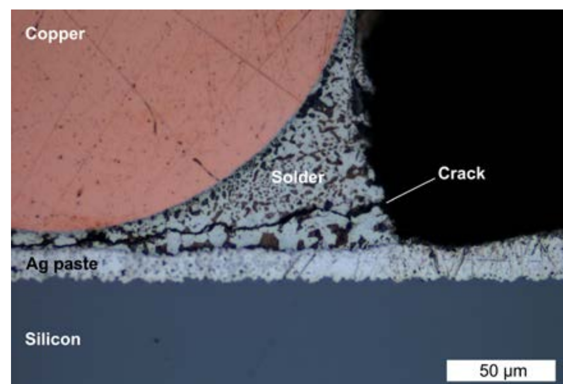

Figure 2: Microsection of a solder joint with a crack in the solder

To understand the mechanical behavior of the MBB front side metallization we simulate the mechanical stress in the solder joints induced during cooling directly after soldering by a model using the finite element method

(FEM). The simulated results are verified with an experiment where the cell bow – as an indicator for mechanical stress of real solar cell samples – is measured by a distance sensor. The required input parameters for the FEM simulation are taken from a detailed material characterization including accurate microscope measurements of the sample geometry as well as literature data of the mechanical parameters for the different module materials involved.

2 MATERIAL CHARACTERIZATION

To characterize the geometry of the simulated solder joints and to determine the mechanical parameters as input for the FEM model, we conduct top view and cross sectional microscope measurements of the solder pads and solder joints and measure the stress strain curves of the used wires with a tensile tester. The physical dimensions of the cell metallization as input parameters for the model are obtained by confocal microscope measurements as shown in table 1.

Table 1: Pad geometry determined by confocal microscope measurements

Pad	Length [µm]	Width [µm]	Height [µm]
Pad 1, 16	2000	1000	21.6
Pad 2 - 15	450	1000	21.6

The geometry of the small pads, the fingers and the redundancy fingers are shown in figure 3.

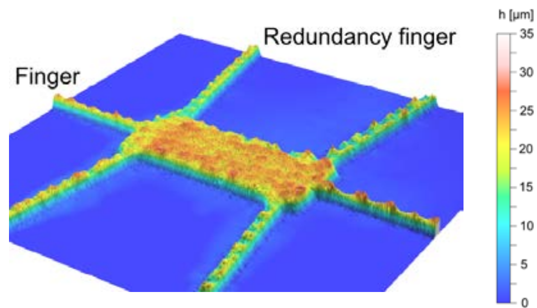

Figure 3: Pseudo-coloured confocal microscope image of the topography of a solder pad on the front side of a MBB solar cell.

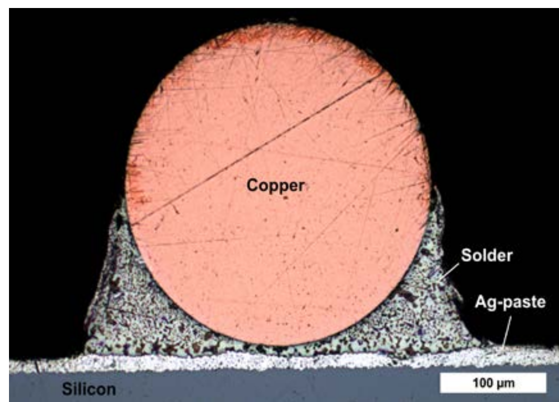

Figure 4: Microsection of a solder joint that shows the copper wire with a diameter of 300 µm, the solder, the screen-printed solder pad consisting of Ag-paste and the silicon.

Microsections of numerous solder joints are prepared and measured to determine the precise layer dimensions of the metallization, the thickness of the silicon and the shape and distribution of the solder (e.g. figure 4).

The used copper wires consist of a copper core (Cu-ETP1) with a diameter of 250, 300 or 430 µm and a solder coating ($Sn_{62}Pb_{36}Ag_2$) with a thickness of 10 to 15 µm. The mechanical properties of copper depend on the manufacturing process and the mechanical treatment directly before the soldering process [6]. The stress-strain curves of commercially available wires and of 1% pre-stretched wires are determined with standard tensile tests according to DIN EN ISO 6892-1 [7]. The pre-stretching is also performed with a tensile testing machine to enable reproducible pre-stretching for every sample.

From the measured engineering stress σ and strain ε the true stress σ_T and strain ε_T are calculated according to equations 1 and 2 [8].

$$\sigma_T = \sigma \cdot (1+\varepsilon) \quad 1$$

$$\varepsilon_T = \ln(1+\varepsilon) \quad 2$$

Figure 5 shows a stress-strain curve (true stress and true strain) of an initial copper wire with 300 µm diameter.

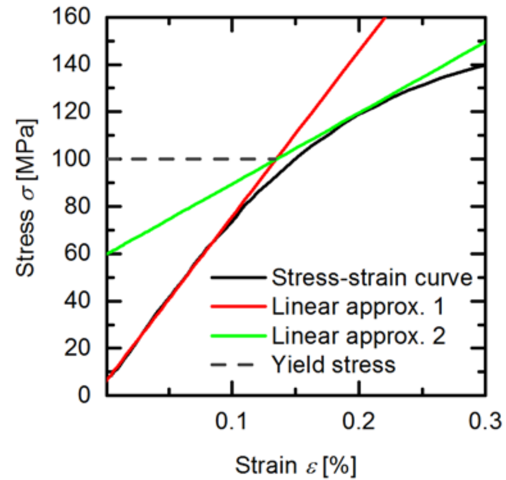

Figure 5: True stress-true strain curve calculated from the measured engineering stress and strain. The gradients of approximation 1 delivers the Young's modulus, the gradient of approximation 2 is assumed as the hardening gradient and the intersection point gives the yield stress.

By means of a bilinear material model [8] the Young's modulus, the yield strength and the hardening gradient are determined from the true stress-strain curve below 0.3 % strain, which is the expected maximum strain an interconnector is stretched due to the mismatch of the coefficients of thermal expansion (CTEs) of copper and silicon in the investigated loading configuration. The results are listed in table 2, showing a slight increase of the Young's modulus and significantly higher yield strength and hardening gradient for the pre-stretched wires, which is caused by cold hardening.

Table 2: Mechanical parameters of the copper wires determined by a bilinear fit of the measured stress-strain curves

Bilinear model Wire diameter [µm]	Young's modulus [GPa]	Yield strength [MPa]	Hardening gradient [GPa]
250	77	120	38
250, 1% pre-streched	80	155	41
300	70	100	30
300, 1% pre-streched	74	120	35
430	67	80	30
430, 1% pre-streched	67	114	34

A summary of the mechanical parameters of the other materials (cell, printed paste and solder), which are taken from literature and used as input parameters for the simulation, is shown in table 3. The CTEs of the materials used in the model are shown in table 4.

Table 3: Mechanical input parameters of the cell material

Material	Young's modulus [GPa]	Yield strength [MPa]	Hardening gradient [GPa]
Bilinear material model			
Aluminum paste	6 [9, 10]	28.3 [10]	0.06[1]
Linear material model			
$Sn_{62}Pb_{36}Ag_2$	16 [11]		
Silver paste	7 [9, 10]		
Silicon	Stiffness Matrix[2] [12]		

[1]Assumption of a moderate growth of the stress when increasing the strain level above the yield point
[2]The Material model for silicon includes an anisotropic Young's modulus

Table 4: CTEs of the solder joint materials

Materials	CTE $[10^{-6} \cdot K^{-1}]$
Copper	17.0 [10]
Aluminum paste	15.9 [9, 10]
$Sn_{62}Pb_{36}Ag_2$	23.9 [11]
Silver paste	10.0 [9, 10]
Silicon	Value table[1] [13]

[1]The Material model for silicon includes temperature dependency of the CTE

3 FINITE ELEMENT MODEL

To simulate the distribution of the mechanical stress in the cell and the solder joint after soldering for MBB front side metallization, the geometry in the developed model consists of a section of the silicon wafer (78 mm x 10 mm x 174.6 µm) with a 29.3 µm thick, homogenous aluminum layer on the rear side and eight silver contact pads on the front side (the pad dimensions are shown in table 1). We assume the influence of the contact and redundancy fingers to be negligible for the cell bow. Hence, by omitting the fingers the model complexity is significantly reduced. For the model the symmetry of the sample along the wire direction is exploited. The simulation mesh consists of tetrahedrals and prisms. Figure 6 shows a detail of the simulated solder joint geometry and the simulation mesh.

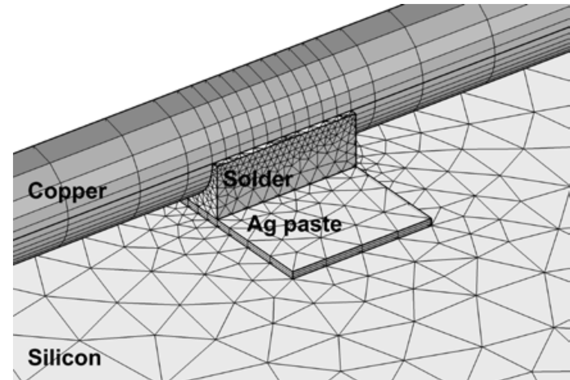

Figure 6: Image of the geometry of the solder joint used for the model and its mesh elements.

During the soldering process with a soldering iron set to 220 °C a temperature of around 170 °C is measured on the cell surface. We therefore start the simulation at 170 °C, which is the assumed stress-free state, and reduce the temperature in steps of 1 °C until 20 °C is reached. Figure 7 shows the simulated deformation and the stress distribution of a sample at 20 °C.

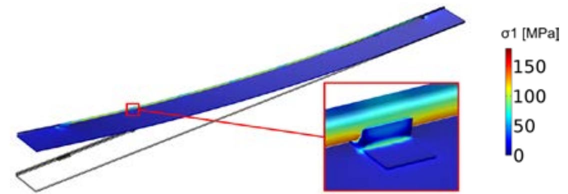

Figure 7: Exemplary simulation result of the cell deformation and the first principle stress (color scheme) of a cell section after cooling from 170 °C to 20 °C.

Figure 8 shows the distribution of the first principle stress σ_I in a longitudinal section of a solder joint. The stress in the aluminum layer on the backside of the cell is below 50 MPa. The minimum stress is located in the silicon. The highest stress occurs in the copper wire and has his maximum at the edge of a contact pad. With increasing distance to the contact pad, the stress in the copper wire decreases.

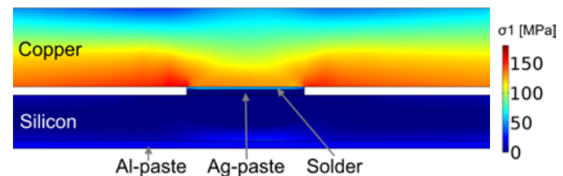

Figure 8: Distribution of the first principle stress (color scheme) in a solder joint (longitudinal section through pad 2) after cooling from 170 °C to 20 °C.

4 EXPERIMENTAL VERIFICATION

To verify the modeling results, solar cell samples with the dimensions of the simulated geometry are prepared. The wires are fluxed (Kester 952-S) and the samples are soldered on a hotplate with a pre-heating temperature of 175 °C and a temperature of the soldering iron of 220 °C. After removing a sample from the hotplate, it cools down to 20 °C and the cell bow becomes measurable as shown in figure 9.

Figure 9: Cell section after cooling to 20 °C for bow measurement using the set up shown in figure 10

The vertical displacement of each sample, as a result of the stress induced by soldering, is measured with a confocal sensor for optical distance measurement as shown in figure 10. The measurement is performed on the back side of the cell section because of its anti-reflex structures on the front side.

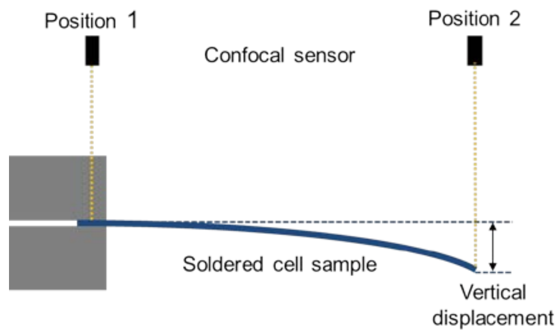

Figure 10: Schematic drawing of the set-up to measure the maximum vertical displacement caused by cell bowing after soldering.

A comparison of the simulation results for the cell displacement and the experimental data are shown in figure 11.

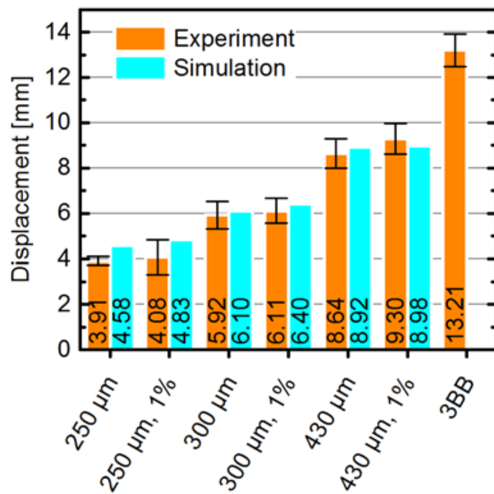

Figure 11: Mean value (orange) and standard deviation (error bars) of the measured vertical displacement for cell samples soldered with commercial available and 1% pre-stretched wires, compared to the simulated vertical displacement (blue bars). The mean value of the measured bow of 3 busbar samples is also included.

It is shown that the results of the simulation are in good agreement with the measured data, especially when using 300 µm or 430 µm wires. The number of the samples we characterized for each wire type and the relative deviation of the simulation from the measurement are summarized in table 5.

Table 5: Number of soldered samples and relative deviation of the simulated cell displacement from the measured experimental data

Wire connector	Sample number	Relative deviation [%]
250 µm	13	+17
250 µm, 1%	12	+18
300 µm	31	+3
300 µm, 1%	32	+5
430 µm	11	+3
430 µm, 1%	12	-3
3BB	11	

The simulation results and the experimental data show that the bow of the cell samples rises when the wire diameter is increased. The largest bow (Mean value of 13.21 mm) show the standard three busbar (3BB) samples soldered with flat wires (Cross-section area: 1500 x 200 µm²). The lower Young's moduli and yield strengths of the thick wires cannot compensate the bow induced by the larger amount of copper of such wires. The results also demonstrate that there is only a slight influence of the pre-stretching (up to 1%) on the cell bow.

5 CONCLUSION AND OUTLOOK

In this work a simulation model for a soldered cell section with Multi Busbar interconnection is designed and experimentally verified. The simulated deformation of the soldered cell samples with MBB interconnection is in good agreement with the measured vertical displacement of the solar cell samples in the experiment. This confirms the assumptions of the finite element model and the used material data. The results of the simulation deliver the stress distribution in a solder joint of the cell samples and enable the identification of maximum stress areas. Potential defects due to the thermo-mechanical stress caused by the soldering process are most likely found where the highest stress values are located.

The presented investigation serves as a basis for future modeling of MBB solar cells soldered on both sides simultaneously and for analyzing the thermo-mechanical stress distribution caused by the CTE mismatch. Additionally, the modeling of conventional busbar cells will allow a direct comparison of the solder induced stresses to the MBB concept.

6 REFERENCES

[1] Söderström, T., P. Papet, and J. Ufheil. "Smart wire connection technology." 28th Eur. Photovoltaic Solar Energy Conf. Exhib., Paris, France, Sep. 2013.

[2] J. Walter, M. Tranitz, M. Volk, C. Ebert, and U. Eitner, "Multi-wire Interconnection of Busbar-free Solar Cells," Energy Procedia, vol. 55, pp. 380-388, 2014.

[3] S. Braun, G. Hahn, and R. Nissler, "Multi-Busbar solar cells and modules: high efficiencies and low silver consumption," presented at the Silicon PV 2013, Hamelin, Germany, 2013.

[4] S. Schindler, J. Schneider, C. Poenisch, R. Nissler, D. Habermann, “Soldering process and material characterization of miniaturized contact structures of a newly developed multi busbar cell metallization concept”, EUPVSEC, 2013.
[5] DIN EN 61215 (VDE 0126-31): Terrestrische Photovoltaik-(PV)-Module mit Silizium-Solarzellen– Bauarteignung und Bauartzulassung (IEC 61215: 2005), International Electrotechnical Commission IEC.
[6] R. Meier, M. Pander, R. Klengel, S. Dietrich, S. Klengel, M. Ebert, and J. Bagdahn, "Reduction of soldering induced stresses in solar cells by microstructural optimization of copper-ribbons," in SPIE Solar Energy+ Technology, 2011, pp. 811206-1 - 811206-13.
[7] ISO, EN 6892-1: 2009, Metallic materials–Tensile testing-Part, vol. 1, 2009.
[8] J. Rösler, H. Harders, and M. Bäker. “Mechanisches Verhalten der Werkstoffe”. Leipzig: Teubner, 2003.
[9] C. Kohn, T. Faber, R. Kübler, J. Beinert, G. Kleer, F. Clement, D. Erath, I. Reis, F. Martin, and A. Müller, "Analyses of warpage effects induced by passivation and electrode coatings in silicon solar cells," in 22nd European Photovoltaic Solar Energy Conference and Exhibition, 2007.
[10] S. Wiese, F. Kraemer, E. Peter, and J. Seib, "Mechanical problems of novel back contact solar modules," in Thermal, Mechanical and Multi-Physics Simulation and Experiments in Microelectronics and Microsystems (EuroSimE), 2012 13th International Conference on, 2012, pp. 1/6-6/6.
[11] Q. Zhang, "Isothermal Mechanical and Thermo-mechanical Durability Characterization of Selected Pb-free Solders," Doctor of Philosophy, Department of Mechanical Engineering, University of Maryland, 2004.
[12] U. Eitner, S. Kajari-Schroeder, M. Koentges, and H. Altenbach, "Thermal stress and strain of solar cells in photovoltaic modules," in Shell-like Structures: Non-classical Theories and Applications. vol. 15, H. Altenbach and V. A. Eremeyev, Eds., ed Berlin/Heidelberg: Springer, 2011.
[13] K. G. Lyon, G. L. Salinger, C. A. Swenson, and G. K. White, "Linear thermal expansion measurements on silicon from 6 to 340 K" Journal of Applied Physics, vol. 48, pp. 865-868, 1977.